

X-RAY VARIABILITY FROM THE ULTRALUMINOUS BLACK HOLE CANDIDATE X-RAY BINARY IN THE GLOBULAR CLUSTER RZ 2109

KRISTEN C. DAGE,¹ STEPHEN E. ZEPF,¹
ARASH BAHRAMIAN,¹ ARUNAV KUNDU,² THOMAS J. MACCARONE,³ MARK B. PEACOCK¹

¹Department of Physics and Astronomy, Michigan State University, East Lansing, MI 48824

²Eureka Scientific, Inc., 2452 Delmer Street, Suite 100 Oakland, CA 94602, USA

³Department of Physics, Box 41051, Science Building, Texas Tech University, Lubbock, TX 79409-1051, USA

ABSTRACT

We present the results of long-term monitoring of the X-ray emission from the ultraluminous X-ray source XMMUJ122939.9+075333 in the extragalactic globular cluster RZ2109. The combination of the high X-ray luminosity, short term X-ray variability, X-ray spectrum, and optical emission suggest that this system is likely an accreting black hole in a globular cluster. To study the long-term behavior of the X-ray emission from this source, we analyze both new and archival *Chandra* and *XMM-Newton* observations, covering 16 years from 2000 to 2016. For all of these observations, we fit extracted spectra of RZ2109 with XSPEC models. The spectra are all dominated by a soft component, which is very soft with typical fit temperatures of $T \simeq 0.15$ keV. The resulting X-ray fluxes show strong variability on short and long timescales. We also find that the X-ray spectrum often shows no significant change even with luminosity changes as large as a factor of five.

Keywords: galaxies: individual (NGC 4472) galaxies: star clusters: individual: RZ 2109 globular clusters: general X-rays: binaries X-rays: galaxies: clusters

1. INTRODUCTION

Determining whether or not globular clusters host black holes, and if so how many and what masses has been the subject of both longstanding interest and current theoretical work (e.g. [Spitzer 1969](#) to [Chatterjee et al. 2017](#)). This interest has grown dramatically with the detection of merging black holes by LIGO ([Abbott et al. 2016b](#)), as black hole mergers in globular clusters are one of the leading possibilities for the origin of the LIGO sources (e.g. [Abbott et al. 2016a](#); [Rodriguez et al. 2016](#)). There is little question black holes are present early in the life of a globular clusters - hundreds to thousands of stellar mass black holes are expected to be produced in typical globular clusters as the result of standard stellar evolution (e.g., [Ivanova et al. 2010a](#)). Early work suggested that dynamical interactions among the black holes may eject many or almost all of them (e.g. [Kulkarni et al. 1993](#), [Sigurdsson & Hernquist 1993](#)). However, recent simulations have found that this process is not as efficient as earlier expectations and current models generally predict the retention of a significant number of black holes in globular clusters (e.g. [Morscher et al. 2015](#), [Heggie & Giersz 2014](#), [Sippel & Hurley 2013](#)).

From an observational perspective, some of the first

and strongest evidence for the presence of black holes in globular clusters has come from X-ray and optical studies of extragalactic globular clusters. One way to find black hole candidates in globular clusters is to identify globular cluster X-ray sources with luminosities in excess of the Eddington limit for an accreting neutron star, which may be indicative of a more massive black hole primary. No such source is found in Galactic globular clusters. However, over the very large sample of extragalactic globular clusters a number of such sources have now been identified in *Chandra* observations of early-type galaxies in the local universe. Because extragalactic globular clusters are unresolved in the X-rays, short term variability in these ultraluminous X-ray sources (ULXs) is critical for eliminating the possibility that the high X-ray luminosity arises from the superposition of multiple accreting neutron stars (e.g., [Kalogera et al. 2004](#)). A handful of such high L_X , variable sources are now known, starting with RZ2109 ([Maccarone et al. 2007](#)), making these among the best candidates for accreting black holes in globular clusters (e.g. [Roberts et al. \(2012\)](#), [Maccarone et al. \(2011\)](#), [Irwin et al. \(2010\)](#) and references therein).

Additional information about these ultraluminous sources can help constrain the nature of the accreting system. For example the source in RZ2109 has strong [OIII]4959,5007 emission with a velocity width of sev-

eral thousand km/s and absolutely no hydrogen observed in emission (Zepf et al. 2008). The strong presence of [OIII]5007 and absence of H β is indicative of accretion from a very O-rich and H-poor donor, for which a CO white dwarf seems most likely (Steele et al. 2014). The broad velocity and high luminosity of the outflow is also consistent with outflows from sources accreting around their Eddington limit, based on both empirical and theoretical work (Zepf et al. 2008, and references therein). Moreover, the [OIII]5007 can not be strongly beamed. Therefore, the lack of similar [OIII] emission in objects without high L_X places valuable limits on any beaming of the X-rays in the RZ2109 source.

It is also interesting to compare the ULXs discovered in globular clusters with the more widely known ULXs in star forming galaxies (see Kaaret et al. (2017) for a review of the latter). While sharing the property of high X-ray luminosity, there are many differences between these populations. The donor stars in the star forming ULX systems are typically high mass stars, while such stars are long dead in globular clusters, and the donor stars in globular cluster systems are either white dwarfs (as in RZ2109, Steele et al. 2014) or other lower mass stars. Moreover, for a ULX in a star forming galaxy the accreting compact object will have been recently formed, and in the case of a neutron star may have an extremely high magnetic field. In contrast, globular clusters have populations of compact objects that formed long ago which can make close binary systems through dynamical interactions within the globular cluster (Ivanova et al. 2010a).

These underlying physical differences may be matched to observational differences between the star forming and globular cluster ULXs. One of the most striking results in the study of ULXs in star forming galaxies is that at least some of the ULXs have accretors that are neutron stars rather than black holes and are thus accreting at many times their formal Eddington limit (e.g. Bachetti et al. 2014, Fürst et al. 2016, Israel et al. 2017b, Israel et al. 2017a). Models to account for these generally involve some combination of extremely large magnetic fields and beaming (review by Kaaret et al. (2017) and references therein). Because most of these models predict that pulses will not be observed at all times and depend on various geometries, it is possible that many ULXs in star forming galaxies are neutron star accretors (King et al. 2017, Middleton & King 2017).

The likely absence of both extreme magnetic fields and substantial beaming differentiates globular cluster ULX sources like RZ2109 from some star forming ULXs and supports identifying the RZ2109 accretor as a black hole (Peacock et al. 2012b). However, studies of ULXs in star forming galaxies provide an extensive set of phenomenological and theoretical work on super-Eddington accretion onto compact objects and its observational manifes-

tations to which observations of RZ2109 can be compared (e.g. Poutanen et al. 2007, Gladstone et al. 2009, Sutton et al. 2013, Middleton et al. 2015). Broadly speaking these papers relate accretion rate relative to Eddington and viewing angle to observed properties such as X-ray spectrum, luminosity, and possible variability based on various assumptions about the underlying astrophysics (see review by Kaaret et al. 2017).

The goal of this paper is to analyze the now large number of X-ray observations of RZ2109 over 16 years, with the aim of constraining the nature of this likely accreting black hole system. RZ2109 is a very well-studied system, with extensive optical spectroscopy (Steele et al. (2014), Steele et al. (2011), Zepf et al. (2008) and references therein), and several extant X-ray studies utilizing Chandra and XMM-Newton. Here we report multiple new Chandra and XMM-Newton observations, and combine these with archival data to study the variability of the X-ray emission from RZ2109 over a broad range of time scales. The paper is arranged so that the observations are presented in Section 2, the results from the analysis of these observation in Section 3, and the conclusions in Section 4.

2. DATA AND ANALYSIS

RZ2109 has been observed numerous times by *XMM-Newton* and *Chandra* observatories over the last 16 years. We reduced and analyzed all of these observations as tabulated in Table 1. The background flare filtered (see further in text for details) *XMM-Newton* net count rates were obtained by filtering the energy in the range 0.3-10 keV in the spectral extraction. We then loaded the spectra into XSPEC, and obtained the net count rates (with no model) by using the show rate command. The *Chandra* source count rates were calculated using funtools¹ to list the counts in the source and background areas based on an image filtered in the 0.3-10 keV range. We then background subtracted the average source counts and divided by the observation length.

2.1. Observations

The *Chandra* observations include both three new datasets we obtained in 2014, 2015, and 2016, and archival data going back to 2000. We used CIAO version 4.9² (Fruscione et al. 2006) for analysis of all *Chandra* data. For most on-axis observations, we manually extracted the spectrum from the source and background regions using `specextract`. For off-axis observations we used ACIS-EXTRACT³ (Broos et al. 2012) to extract the source regions (Broos et al. 2012). Specifically, in observations 12888 and 12889, the source is located on ACIS

¹ <https://github.com/ericmandel/funtools>

² <http://cxc.harvard.edu/ciao/>

³ http://www2.astro.psu.edu/xray/docs/TARA/ae_users_guide.html

Table 1. *Chandra* and background flare filtered *XMM-Newton* observations, background subtracted average source count rates and raw source counts in 0.3-10 keV.

ObsID	Date	Exposure (ks)	Avg. Rate count/s	Src. Counts
322 ^a	2000-03-19	10	4.3×10^{-3}	48
321	2000-06-12	40	8.7×10^{-3}	398
8095	2008-02-23	5	1.1×10^{-2}	60
11274	2010-02-27	40	2.1×10^{-4}	19
12978	2010-11-20	20	9.6×10^{-4}	19
12889	2011-02-14	140	2.4×10^{-3}	425
12888	2011-02-21	160	1.0×10^{-3}	230
16260	2014-08-04	25	3.1×10^{-3}	79
16261	2015-02-24	25	9.0×10^{-5}	3
16262	2016-04-30	25	5.6×10^{-4}	16
0112550601 ^b	2002-06-05	11	2.3×10^{-2}	282
0200130101	2004-01-01	72	4.5×10^{-3}	465
0761630101	2016-01-05	44	2.1×10^{-2}	1147
0761630201	2016-01-07	35	4.3×10^{-4}	29
0761630301	2016-01-09	65	3.9×10^{-4}	217

^aThis observation and below: *Chandra*

^b This observation and below: *XMM-Newton*

chip 8 and thus far off-axis. Additionally in observation 12888, it is located on the edge of this chip and is affected by dithering and edge effects. Given these issues and low signal-to-noise ratio of the detection in these observations, we used ACIS-EXTRACT to extract the spectra. Source extraction regions constructed by ACIS-EXTRACT are polygons approximating *Chandra*-ACIS point spread function based on MARX (Davis et al. 2012) simulations⁴. ACIS-EXTRACT also applies PSF corrections to ancillary response files (ARF) and exposure and background scaling corrections to the spectrum to take into account edge effects.

RZ2109 was also observed with *XMM-Newton* in 2002, 2004, 2008⁵, and three times in 2016 (see Table 1). We used SAS 16.1.0⁶ to extract the spectra from the MOS1, MOS2 and pn detections.

We set FLAG== 0 to screen conservatively⁷, and originally extracted single and double events (pattern <= 4) as recommended for *XMM* pn, however, in observations heavily impacted with flares (0200130101, 0761630201, and 0761630301), we only extracted single events (pattern == 0). For MOS1 and MOS2, we select (pattern<=12). The data was filtered for high back-

⁴ We note that MARX 5.0, 5.1, and 5.2 simulate PSF of off-axis sources inaccurately (see <https://github.com/Chandra-MARX/marx/pull/21>). We have used MARX 5.3.2 for this work, which has addressed this issue.

⁵ Observation 0510011501 did not have enough information left post-background flare filtering and thus is not used in this analysis.

⁶ <https://www.cosmos.esa.int/web/xmm-newton/sas>

⁷ https://heasarc.gsfc.nasa.gov/docs/xmm/hera_guide/node33.html

ground flares by only selecting times at which the background was constant. Those times were determined by examining the background light curve from the PPS. We ignored any counts below 0.2 keV. To account for differences among the three detectors when fitting, a constant factor was added to the best fit models; the value for pn was frozen at 1.0, while the values for MOS1 and MOS2 were free.

We used XSPEC version 12.9.1⁸ (Arnaud 1996) to analyze the X-ray spectra of both new and archival *Chandra* and *XMM-Newton* observations. All XSPEC analysis used the abundance of elements from Wilms et al. (2000).

We used the *F-test* function to compare the χ^2 statistics of a single disk component model with an absorption term to a two component model (disk component added to a powerlaw model pegged from 0.5-8 keV, also with absorption) for the three *Chandra* observations with the highest counts (321, 12888, and 12889). The probability that the improved fit statistics of the two component model is due to chance is respectively: 0.002, 0.006, 1.4e-05. Similarly, the *F-test* probabilities of a single powerlaw model with absorption compared to the absorbed two component model are: 0.047, 0.047 and 0.001. Therefore, we fit a multicolor disk (MCD) model (diskbb) added to a power law `pegpwlw`, and multiplied by the absorption component to all observations. We note for completeness that if a power law is fit as a single-component model to the *Chandra* data, its index is in the range from 3.2 to 4.3, while the *XMM-Newton* data typically have a single-component powerlaw index around 3.0. In all our fits, we include an absorption term, `tbabs`, fixed to a foreground hydrogen column density of $N_H = 1.6 \times 10^{20} \text{ cm}^{-2}$ ⁹. We found no evidence for a second absorption column; we fit the highest count *Chandra* data with a second absorption parameter and found that in each case, the best fit value was consistent with zero.

For the bulk of the observations χ^2 was used as the fitting statistic. Spectra with more than 100 source counts were binned in groups of 20; spectra with fewer counts than that were binned with 1 count per bin and fit with *c-stats* (Cash 1979).

To estimate the unabsorbed fluxes in the 0.5-8keV range we used XSPEC's multiplicative model `cflux`¹⁰ with the best fit spectral model. After adding in the `cflux` component and refitting, we then used the error command in XSPEC on the flux parameter and obtained upper and lower bounds on the fluxes of each observation to the 90% confidence interval. All parameter errors were also obtained in this manner.

While all of our fitting is carried out in the 0.5-8keV range appropriate for *Chandra* data, many X-ray results

⁸ <https://heasarc.gsfc.nasa.gov/xanadu/xspec/>

⁹ <http://cxc.harvard.edu/toolkit/colden.jsp>

¹⁰ <https://heasarc.gsfc.nasa.gov/xanadu/xspec/manual/XSmodelCflux.html>

are given in the 0.2-10 keV range. Therefore to compare to other work, we calculate the 0.2-10 keV fluxes and luminosities based on our spectral fits to the data from 0.5-8 keV, also using `cflux`.

Tables 2 and 3 show best fit parameters, fit statistics and the fitted flux for *Chandra* and *XMM-Newton* observations respectively. The fluxes and fit parameters are also plotted in Figure 1.

Two *Chandra* observations have extremely low average source counts. Maccarone et al. (2010a) have previously found 19 source count rates with a background of 10.8 counts for obsID 11274, which, despite being highly off-axis, is significant at the 95% confidence level (Gehrels 1986). In obsID 16261, we detect three counts in the source region, which - considering the expected scaled background of 1 count - is also significant at the 95% confidence level. To estimate a flux for both of these observations, we took the background subtracted count rates and used PIMMS¹¹ to fit with a powerlaw index of 3.5, which was the common best fit to the single powerlaw model of the other *Chandra* data. *XMM-Newton* observation 0761630201 had very few counts left post background flare filtering. This, in conjunction with a relatively high background ($\simeq 50\%$) meant that detailed spectral analysis was not possible. However, we were able to fit a single component disk model to the data and obtain a flux using `cflux`. This lends significant uncertainty to this flux estimate.

3. RESULTS

The overall goal of this paper is to monitor variations in the X-ray luminosity of RZ2109 over the time covered by all of the available data, ranging from 2000 to 2016. Figure 2 shows the luminosities in the 0.2-10 keV range, which were calculated using the fluxes from Section 2 and a distance of 16.1 Mpc (Macri et al. 1999). The luminosities are also listed in Table 4.

One of the main results apparent from Figure 2 and Table 4 is that RZ2109 varies significantly over all of the time scales observed, from days to years. During some observations RZ2109 is observed to have $L_X \sim 4 \times 10^{39}$ erg s^{-1} , while at other times it is observed to have $L_X \sim 2 - 3 \times 10^{38}$ erg s^{-1} or even fainter, along with various times at which RZ2109 is found to be between these luminosities. This variability is surprising because there is strong evidence in other ways that the source is a stellar mass black hole accreting material from a carbon-oxygen white dwarf at a very high rate, at or somewhat above its formal Eddington limit (e.g., Peacock et al. 2012a; Roberts et al. 2012). In such a case the source is expected to be persistent because accretion disks in high luminosity, short period ultracompacts like this are

not expected to have ionization instabilities (e.g., Maccarone et al. 2010b). While there are beginning to be counter-examples to this argument (see Maccarone et al. 2010b), understanding such systems may give important clues to the formation and accretion processes in these globular cluster black hole sources. It is interesting to compare the variability of RZ2109 to that of other ultraluminous X-ray sources in extragalactic globular clusters. Of the six such sources published - Maccarone et al. (2007), Brassington et al. (2010); Shih et al. (2010); Irwin et al. (2010); Maccarone et al. (2011); Roberts et al. (2012), all vary, with at least three of them varying by more than an order of magnitude. There is a need to be careful about variability in this list, because variability is also one of the criteria to ensure that most of the X-ray flux comes from a single source and not multiple sources in the globular cluster, and variability is one of the criteria used in these papers. However, in these cases, the ultraluminous sources are typically the brightest X-ray sources among the globular cluster sources in each galaxy. So substantial and large variability appears to be the norm for ultraluminous X-ray sources in extragalactic globular clusters.

Given the luminosity variability observed in these sources, it is natural to test whether there is any corresponding spectral variability. A key feature of the variability RZ2109 found here is that there is often *no* evidence for corresponding changes in the X-ray spectra of RZ2109. The similarity of the X-ray spectra at different observed fluxes can be seen in Tables 2 and 3 and Figure 1. This result is different than that found in the original variability discovery for RZ2109 which showed that the decrease in flux seen within the 2002 *XMM-Newton* observation was driven by a decrease in the soft component that can be interpreted as a change in the column density of absorbing material along the line of sight (Maccarone et al. 2007, Shih et al. 2008). While this is still true for the flux change within the 2002 *XMM-Newton* observation, such a model can not explain most of the variability among the many observations shown here. Other ULX sources in extragalactic globular clusters show a range of behavior in the relationship between luminosity and spectral variability. Shih et al. (2010) find a ULX in an extragalactic globular cluster in NGC 1399 with more than a factor of ten decrease in luminosity and no evident change in spectral shape. On the other hand, a different extragalactic globular cluster ULX in NGC 4649 studied by Roberts et al. (2012) does exhibit spectral changes in some observations. The overall picture is that some spectral variability happens, but there are clear observations in multiple sources of little or no spectral variability even with order of magnitude luminosity changes.

It is also natural to ask whether there is any overall longterm trend of L_X with time for RZ2109. Unfor-

¹¹ <http://cxc.harvard.edu/toolkit/pimms.jsp>

Table 2. *Chandra* Fit Parameters and Fluxes (0.5-8 keV) for XSPEC best fit model `tbabs*(diskbb+pegpwlw)`. Hydrogen column density (N_H) frozen to $1.6 \times 10^{20} \text{ cm}^{-2}$.

Date	T_{in} (keV)	Disk Norm ^a	Γ	Powerlaw Flux ($\text{erg cm}^2 \text{ s}^{-1}$)	$\chi^2/\text{d.o.f.}$ ^b	Unabsorbed Flux ($\text{erg cm}^2 \text{ s}^{-1}$)
2000-03-19	0.11 $^{+0.04}_{-0.03}$	107 $^{+670}_{-90}$	1.3 $^{+1.2}_{-1.1}$	$3.0(^{+2.5}_{-1.4}) \times 10^{-14}$	N/A ^c	$5.7(^{+2.4}_{-1.6}) \times 10^{-14}$
2000-06-12	0.12 ± 0.02	68 $^{+85}_{-34}$	1.7 ± 0.5	$3.8(\pm 0.8) \times 10^{-14}$	3.14/16	$7.0 (\pm 0.9) \times 10^{-14}$
2008-02-23	0.13 $^{+0.03}_{-0.02}$	60 $^{+164}_{-42}$	0.5 $^{+1.4}_{-2.5}$	$2.2(^{+2.7}_{-1.8}) \times 10^{-14}$	N/A ^d	$4.5(^{+1.2}_{-1.0}) \times 10^{-14}$
2010-02-27 ^e	—	—	(3.5) ^f	$9.2 (^{+10.0}_{-6.2}) \times 10^{-16}$	—	$9.2(^{+10.0}_{-6.2}) \times 10^{-16}$
2010-11-20	0.13 $^{+0.08}_{-0.04}$	3.1 $^{+38.3}_{-2.9}$	0.2 $^{+1.6}_{-2.1}$	$6.7 (^{+10.0}_{-4.5}) \times 10^{-15}$	N/A ^g	$9.6(^{+8.8}_{-4.6}) \times 10^{-15}$
2011-02-14	0.13 ± 0.02	21 $^{+36}_{-14}$	1.3 ± 0.6	$1.9 (\pm 0.4) \times 10^{-14}$	1.19/16	$3.6(\pm 0.4) \times 10^{-14}$
2011-02-21	0.11 ± 0.03	30 $^{+135}_{-23}$	1.8 ± 0.6	$1.0 (\pm 0.2) \times 10^{-14}$	1.69/7	$1.6(\pm 0.3) \times 10^{-14}$
2014-08-04	0.12 $^{+0.04}_{-0.03}$	39 $^{+233}_{-34}$	2.0 ± 0.7	$2.6(\pm 0.8) \times 10^{-14}$	N/A ^h	$2.8(^{+0.6}_{-0.5}) \times 10^{-14}$
2015-02-24 ⁱ	—	—	(3.5)	$9.3(^{+27.7}_{-7.9}) \times 10^{-16}$	—	$9.3(^{+27.7}_{-7.9}) \times 10^{-16}$
2016-04-30	0.09 ± 0.05	242 $^{2169}_{-239}$	1.8 $^{+1.5}_{-1.6}$	$6.9(^{+5.0}_{-3.5}) \times 10^{-15}$	N/A ^j	$2.0(^{+1.1}_{-0.8}) \times 10^{-14}$

^a $(R_{in}/D_{10})^2 \cos\theta$ ^bReduced χ^2 per degree of freedom^cToo few data points for χ^2 statistics. Pearson χ^2 : 80.63 using 41 PHA bins.^dToo few data points for χ^2 statistics. Pearson χ^2 : 570.25 using 44 PHA bins.^eCount rate from [Maccarone et al. \(2010a\)](#), fit with PIMMS.^fBest fit powerlaw index from single component powerlaw model.^gToo few data points for χ^2 statistics. Pearson χ^2 : 20.99 using 22 PHA bins.^hToo few data points for χ^2 statistics. Pearson χ^2 : 86.80 using 64 PHA bins.ⁱMarginal detection—fit with PIMMS.^jToo few data points for χ^2 statistics. Pearson χ^2 : 12.07 using 16 PHA bins.**Table 3.** *XMM-Newton* Fit Parameters and Fluxes (0.5-8 keV) for XSPEC model `tbabs*(diskbb+pegpwlw)`. Hydrogen column density (N_H) frozen to $1.6 \times 10^{20} \text{ cm}^{-2}$.

Date	CCF Constant pn/MOS1/MOS2	T_{in} (keV)	Disk Norm ^a	Γ	Powerlaw Flux ($\text{erg cm}^2 \text{ s}^{-1}$)	$\chi^2/\text{d.o.f.}$ ^b	Unabsorbed Flux ($\text{erg cm}^2 \text{ s}^{-1}$)
2002-06-05	(1.0)/1.20/0.83	0.14 $^{+0.06}_{-0.02}$	18 $^{+25}_{-16}$	2.6 $^{+0.7}_{-3.9}$	$3.9 (\pm 1.5) \times 10^{-14}$	1.73/16	$6.3 (^{+3.8}_{-1.0}) \times 10^{-14}$
2004-01-01 ^c	(1.0)/1.57/1.59	0.17 ± 0.02	1.8 $^{+0.8}_{-0.5}$	0.6 $^{+0.7}_{-0.9}$	$9.2(^{+3.7}_{-3.4}) \times 10^{-15}$	2.31/45	$1.7 (\pm 0.4) \times 10^{-14}$
2016-01-05	(1.0)/0.85/1.08	0.16 ± 0.01	7.2 $^{+2.6}_{-1.8}$	1.0 ± 0.4	$2.7 (\pm 0.5) \times 10^{-14}$	1.38/56	$5.0 (\pm 0.6) \times 10^{-14}$
2016-01-07	—	—	—	—	—	—	$8.9(^{+13.0}_{-8.2}) \times 10^{-16}$
2016-01-09	N/A ^d	0.15 $^{+0.15}_{-0.02}$	0.2 $^{+1.4}_{-0.1}$	1.4 $^{+1.4}_{-0.6}$	$\leq 7.0 \times 10^{-15}$	0.59/6	$2.3(^{+5.2}_{-2.2}) \times 10^{-15}$

^a $(R_{in}/D_{10})^2 \cos\theta$ ^bReduced χ^2 per degree of freedom^cPN detection started 3ks after MOS detectors^dToo few counts in MOS1 & MOS2, used pn only

Unfortunately the data are not quite adequate for addressing this question specifically. It is intriguing that many of the fainter fluxes appear to be found at more recent times. However, there are observations in 2014 and 2016 in which $L_X \simeq 3 \times 10^{39}$ erg s $^{-1}$, and thus well within the ULX regime and not much different than observations in 2000 and 2002. Given the short term variability clearly evident in RZ2109, one way to get at the long-term changes in RZ2109 may be to study its [OIII]5007 emission which appears to be emitted over a region of light months to light years, and therefore samples the overall photoionizing flux averaged over those timescales (Peacock et al. 2012b). The physical origin of the variability RZ2109 has not yet been established. As noted above, the accretion disk is not expected to be subject to ionization instabilities, so a different mechanism must be operating.

One natural mechanism to produce changes in the accretion rate over time is to have small changes in the eccentricity of the orbit (e.g., Hut & Paczynski 1984), perhaps due to the Kozai mechanism (Kozai 1962), in which a lower mass third star in an outer orbit introduces eccentricity into the main two body system. For typical parameters for an RZ2109-like system and a mass of the third star of $0.5M_\odot$, the Kozai timescale is roughly a decade. This therefore may account for any long term trend we may see in RZ2109, but not very short term variability. This is why it was attractive originally to try to explain RZ2109’s variability with varying absorption, but such an explanation fails to account for the absence of spectral changes seen in many datasets since. Other possibilities for short-term variability are listed in the Maccarone et al. (2010b) study of similar variability of the Galactic ultracompact binary 4U 0513–40. These possibilities include tidal disc instabilities (e.g., Whitehurst 1988; Osaki 1995) and irradiation of the donor star leading to modulations of the accretion rate (e.g., Hameury et al. 1986). It is not yet clear whether these can account for variability observed in RZ2109.

The observed X-ray spectrum and variability of RZ2109 can also be compared to the well-known ULXs observed in star forming galaxies (Kaaret et al. 2017). Compared to most of these ULXs not in globular clusters, RZ2109 is significantly softer and much more variable. Within the field ULX population, there is a class of objects known as ultrasoft ULXs (ULSs) that are both softer and more variable than most ULXs (e.g., Earnshaw & Roberts 2017; Urquhart & Soria 2016). These papers also find that the variability in ULSs is primarily at higher X-ray energies, although there is an exception to this general characteristic (Feng et al. 2016). Thus RZ2109 differs from most field ULSs in that its variability is either mostly at low energies (e.g., Shih et al. 2008), or the luminosity varies equally at all energies, as shown

above.

That the globular cluster ULXs are different than most ULXs in star forming galaxies is not surprising. Globular cluster ULXs are essentially low-mass X-ray binaries (LMXBs) and nearly all field ULXs are high mass X-ray binaries (HMXBs). The binaries that make the globular cluster ULXs are also likely to be formed by dynamical interactions within the globular cluster (Ivanova et al. 2010b), unlike the binary stellar evolution that makes field ULXs. As a result, the accretor in globular cluster ULXs is likely to be much older and thus not have the large magnetic fields often proposed for field ULXs. Differences in the donor stars will also be significant in globular cluster ULXs compared to field ULXs. Globular cluster sources will have old, low-mass donors while star forming ULXs typically have young, higher mass donors. This leads to differences in the orbital parameters and the composition of the accreted material, among others, which then may have implications for the resulting observables in the ULXs.

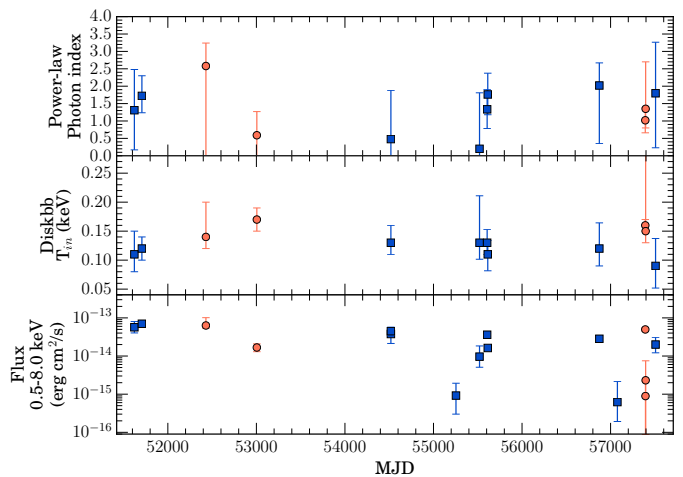


Figure 1. Top panel shows best fit powerlaw index for *Chandra* and *XMM* observations, middle panel shows disk temperature, lowest panel shows calculated unabsorbed model flux. *Chandra* data is represented by blue squares, and the *XMM-Newton* data by orange circles. All parameters and fluxes are in the 0.5–8 keV band.

4. CONCLUSIONS

We confirm long-term variability in the X-ray emission from the globular cluster black-hole candidate source XMMUJ122939.9+075333 in the extragalactic globular cluster RZ2109. The system shows strong luminosity variability over long and short time scales, dropping anywhere from as low as $L_X \simeq 7 \times 10^{37}$ erg s $^{-1}$ to as high as $L_X \simeq 5 \times 10^{39}$ erg s $^{-1}$. The system also underwent significant changes in luminosity over very short time scales: observations four days apart from each other showed a

Table 4. All luminosities in 0.2-10 keV.

Date	Luminosity (erg s^{-1})	Lower Bound (erg s^{-1})	Upper Bound (erg s^{-1})	Obs
2000-03-19	4.0×10^{39}	2.9×10^{39}	5.6×10^{39}	Chandra
2000-06-12	4.4×10^{39}	3.9×10^{39}	6.0×10^{39}	Chandra
2002-06-05	4.9×10^{39}	4.4×10^{39}	5.5×10^{39}	XMM
2004-01-01	1.0×10^{39}	8.4×10^{38}	1.3×10^{39}	XMM
2008-02-23	4.7×10^{39}	3.3×10^{39}	7.0×10^{39}	Chandra
2010-02-27	7.4×10^{37}	1.1×10^{38}	1.3×10^{38}	Chandra
2010-11-20	5.5×10^{38}	2.7×10^{38}	1.2×10^{39}	Chandra
2011-02-14	2.1×10^{39}	1.8×10^{39}	2.5×10^{39}	Chandra
2011-02-21	1.1×10^{39}	8.7×10^{38}	1.3×10^{39}	Chandra
2014-08-04	2.7×10^{39}	2.0×10^{39}	3.3×10^{39}	Chandra
2015-02-24	6.3×10^{37}	9.8×10^{36}	2.74×10^{38}	Chandra
2016-01-05	3.1×10^{39}	2.8×10^{39}	3.4×10^{39}	XMM
2016-01-07	5.2×10^{38}	4.9×10^{38}	5.6×10^{38}	XMM
2016-01-09	3.5×10^{37}	6.1×10^{36}	7.4×10^{37}	XMM
2016-04-30	1.2×10^{38}	2.0×10^{37}	3.7×10^{38}	Chandra

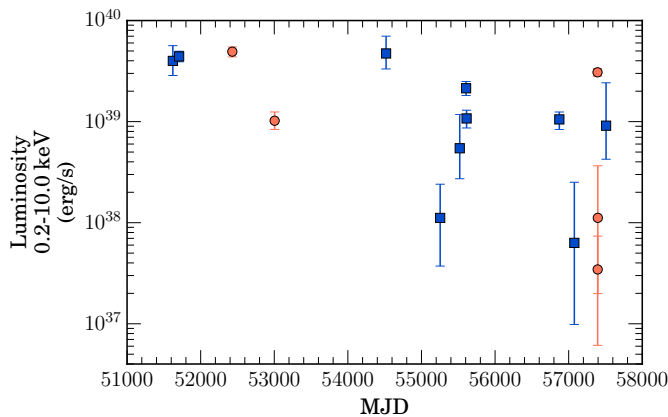


Figure 2. Luminosity variability of RZ2109 in energy band 0.2-10.0 keV. *Chandra* data is represented by blue squares, and the *XMM-Newton* data by orange circles.

drop in luminosity by almost a factor of five. Over 16 years of X-ray monitoring, the spectral shape remains extremely soft. The fitted *Chandra* and *XMM-Newton* spectra for the high count observations can be seen in the appendix. While the fit quality is too low to make any statements in regards to spectral variability, it is remarkable how consistently soft the spectra are.

KCD, SEZ, and MBP acknowledge support from Chandra grant GO4-15089A. SEZ and MBP also acknowledge support from the NASA ADAP grant NNX15AI71G. This research has made use of data obtained from the Chandra Data Archive and the Chandra Source Catalog, and is based on observations obtained with XMM-Newton, an ESA science mission with instruments and contributions directly funded by ESA Member States and NASA. We also acknowledge use of NASA’s Astrophysics

Data System and Arxiv.

Software: The following softwares and packages were used for analysis: CIAO, software provided by the Chandra X-ray Center (CXC), HEASOFT obtained from the High Energy Astrophysics Science Archive Research Center (HEASARC), a service of the Astrophysics Science Division at NASA/GSFC and of the Smithsonian Astrophysical Observatory’s High Energy Astrophysics Division, SAS, the XMM-Newton Science Analysis System, SAOImage DS9, developed by Smithsonian Astrophysical Observatory, NUMPY (Van Der Walt et al. 2011), MATPLOTLIB (Hunter 2007) and ASTROPY (Astropy Collaboration et al. 2013).

APPENDIX

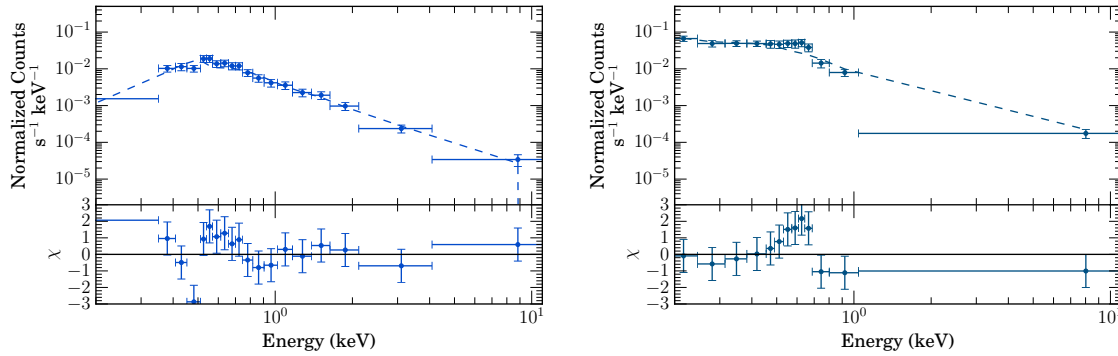


Figure 3.: Left: Fitted spectrum with residuals of *Chandra* ObsID 321 (2000-06-12). Right: Fitted spectrum with residuals of *XMM-Newton* observation 0112550601 (2002-06-05, pn only).

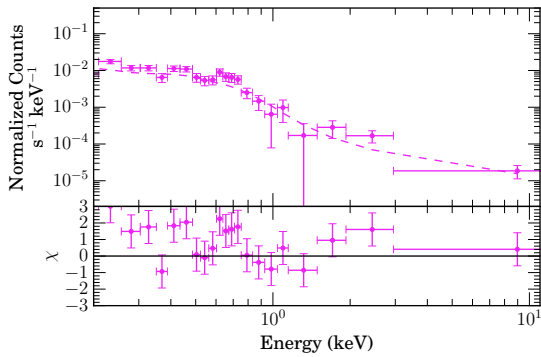


Figure 4.: Left: Fitted spectrum with residuals of *XMM-Newton* observation 0200130101 (2004-01-01, pn only).

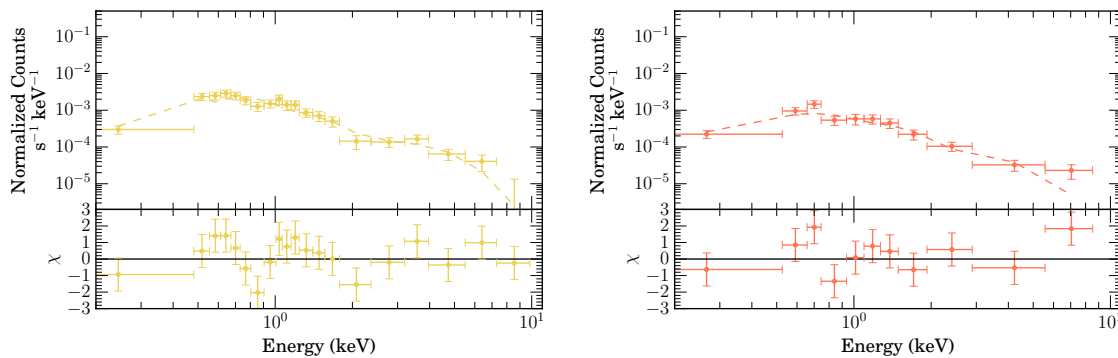


Figure 5.: Left: Fitted spectrum with residuals of *Chandra* ObsID 12889 (2011-02-14). Right: Fitted spectrum with residuals of *Chandra* ObsID 12888 (2011-02-21).

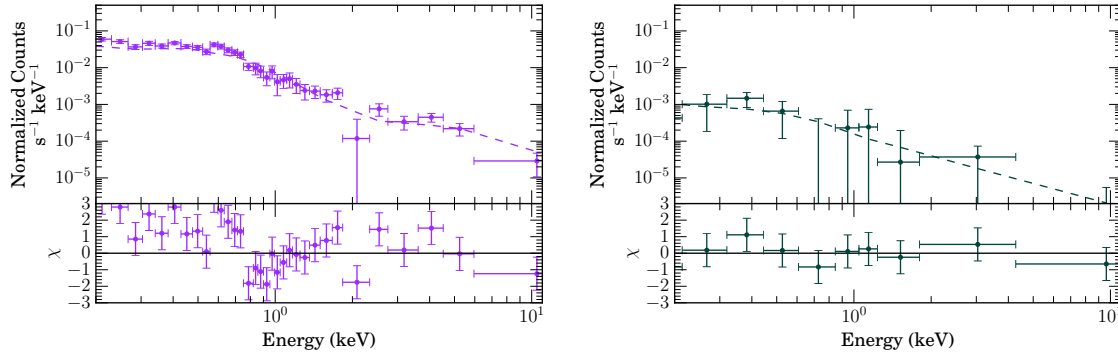


Figure 6.: Left: Fitted spectrum with residuals of *XMM-Newton* observation 0761630101 (2016-01-05, pn only). Right: Fitted spectrum with residuals of *XMM-Newton* observation 0761630301 (2016-01-09, pn only).

REFERENCES

- Abbott, B. P., Abbott, R., Abbott, T. D., et al. 2016a, *ApJL*, 818, L22
- . 2016b, *Physical Review Letters*, 116, 061102
- Arnaud, K. A. 1996, in *Astronomical Society of the Pacific Conference Series*, Vol. 101, *Astronomical Data Analysis Software and Systems V*, ed. G. H. Jacoby & J. Barnes, 17
- Astropy Collaboration, Robitaille, T. P., Tollerud, E. J., et al. 2013, *A&A*, 558, A33
- Bachetti, M., Harrison, F. A., Walton, D. J., et al. 2014, *Nature*, 514, 202
- Brassington, N. J., Fabbiano, G., Blake, S., et al. 2010, *ApJ*, 725, 1805
- Broos, P., Townsley, L., Getman, K., & Bauer, F. 2012, *AE: ACIS Extract*, *Astrophysics Source Code Library*, ascl:1203.001
- Cash, W. 1979, *ApJ*, 228, 939
- Chatterjee, S., Rodriguez, C. L., Kalogera, V., & Rasio, F. A. 2017, *ApJL*, 836, L26
- Davis, J. E., Bautz, M. W., Dewey, D., et al. 2012, in *Proc. SPIE*, Vol. 8443, *Space Telescopes and Instrumentation 2012: Ultraviolet to Gamma Ray*, 84431A
- Earnshaw, H. M., & Roberts, T. P. 2017, *MNRAS*, 467, 2690
- Feng, H., Tao, L., Kaaret, P., & Grisé, F. 2016, *ApJ*, 831, doi:10.3847/0004-637X/831/2/117
- Fruscione, A., McDowell, J. C., Allen, G. E., et al. 2006, in *Proc. SPIE*, Vol. 6270, *Society of Photo-Optical Instrumentation Engineers (SPIE) Conference Series*, 62701V
- Fürst, F., Walton, D. J., Harrison, F. A., et al. 2016, *ApJL*, 831, L14
- Gehrels, N. 1986, *ApJ*, 303, 336
- Gladstone, J. C., Roberts, T. P., & Done, C. 2009, *MNRAS*, 397, 1836
- Hameury, J. M., King, A. R., & Lasota, J. P. 1986, *A&A*, 162, 71
- Heggie, D. C., & Giersz, M. 2014, *MNRAS*, 439, 2459
- Hunter, J. D. 2007, *Computing in Science and Engineering*, 9, 90
- Hut, P., & Paczynski, B. 1984, *ApJ*, 284, 675
- Irwin, J. A., Brink, T. G., Bregman, J. N., & Roberts, T. P. 2010, *ApJL*, 712, L1
- Israel, G. L., Belfiore, A., Stella, L., et al. 2017a, *Science*, 355, 817
- Israel, G. L., Papitto, A., Esposito, P., et al. 2017b, *MNRAS*, 466, L48
- Ivanova, N., Chaichenets, S., Fregeau, J., et al. 2010a, *ApJ*, 717, 948
- . 2010b, *ApJ*, 717, 948
- Kaaret, P., Feng, H., & Roberts, T. P. 2017, *ARA&A*, 55, 303
- Kalogera, V., King, A. R., & Rasio, F. A. 2004, *ApJL*, 601, L171
- King, A., Lasota, J.-P., & Kluźniak, W. 2017, *MNRAS*, 468, L59
- Kozai, Y. 1962, *AJ*, 67, 591
- Kulkarni, S. R., Hut, P., & McMillan, S. 1993, *Nature*, 364, 421
- Maccarone, T. J., Kundu, A., Zepf, S. E., & Rhode, K. L. 2007, *Nature*, 445, 183
- . 2010a, *MNRAS*, 409, L84
- . 2011, *MNRAS*, 410, 1655
- Maccarone, T. J., Long, K. S., Knigge, C., Dieball, A., & Zurek, D. R. 2010b, *MNRAS*, 406, 2087
- Macri, L. M., Huchra, J. P., Stetson, P. B., et al. 1999, *ApJ*, 521, 155
- Middleton, M. J., & King, A. 2017, *MNRAS*, 470, L69
- Middleton, M. J., Walton, D. J., Fabian, A., et al. 2015, *MNRAS*, 454, 3134
- Morscher, M., Pattabiraman, B., Rodriguez, C., Rasio, F. A., & Umbreit, S. 2015, *ApJ*, 800, 9
- Osaki, Y. 1995, *PASJ*, 47, L11
- Peacock, M. B., Zepf, S. E., & Maccarone, T. J. 2012a, *ApJ*, 752, 90
- Peacock, M. B., Zepf, S. E., Kundu, A., et al. 2012b, *ApJ*, 759, 126
- Poutanen, J., Lipunova, G., Fabrika, S., Butkevich, A. G., & Abolmasov, P. 2007, *MNRAS*, 377, 1187
- Roberts, T. P., Fabbiano, G., Luo, B., et al. 2012, *ApJ*, 760, 135
- Rodriguez, C. L., Chatterjee, S., & Rasio, F. A. 2016, *Phys. Rev. D*, 93, 084029
- Shih, I. C., Kundu, A., Maccarone, T. J., Zepf, S. E., & Joseph, T. D. 2010, *ApJ*, 721, 323
- Shih, I. C., Maccarone, T. J., Kundu, A., & Zepf, S. E. 2008, *MNRAS*, 386, 2075
- Sigurdsson, S., & Hernquist, L. 1993, *Nature*, 364, 423
- Sippel, A. C., & Hurley, J. R. 2013, *MNRAS*, 430, L30
- Spitzer, Jr., L. 1969, *ApJL*, 158, L139
- Steele, M. M., Zepf, S. E., Kundu, A., et al. 2011, *ApJ*, 739, 95
- Steele, M. M., Zepf, S. E., Maccarone, T. J., et al. 2014, *ApJ*, 785, 147
- Sutton, A. D., Roberts, T. P., & Middleton, M. J. 2013, *MNRAS*, 435, 1758
- Urquhart, R., & Soria, R. 2016, *MNRAS*, 456, 1859
- Van Der Walt, S., Colbert, S. C., & Varoquaux, G. 2011, *ArXiv e-prints*, arXiv:1102.1523
- Whitehurst, R. 1988, *MNRAS*, 232, 35
- Wilms, J., Allen, A., & McCray, R. 2000, *ApJ*, 542, 914
- Zepf, S. E., Stern, D., Maccarone, T. J., et al. 2008, *ApJL*, 683, L139